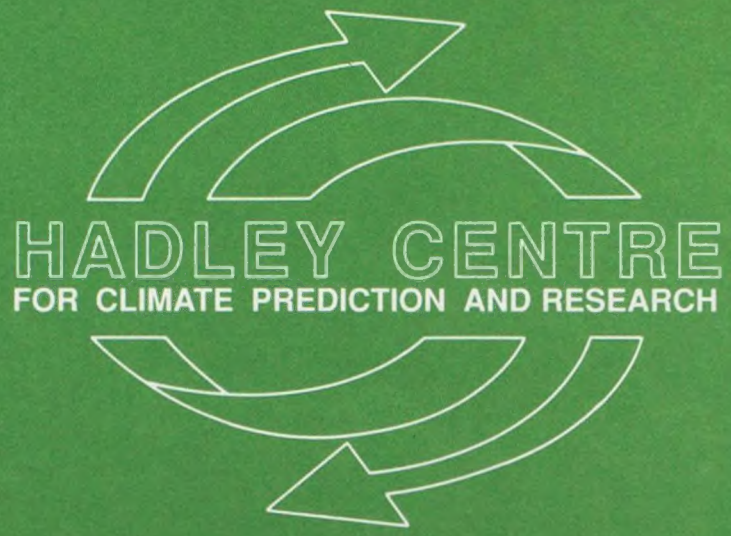

Coupled Tropical ocean global atmosphere models at the UKMO

by

M. K. Davey, C. Gordon, S. Ineson and S. Lawrence

CRTN 21 December 1991

CLIMATE
RESEARCH
TECHNICAL
NOTE

Hadley Centre
Meteorological Office
London Road
Bracknell
Berkshire RG12 2SY

CLIMATE RESEARCH TECHNICAL NOTE NO. 21

COUPLED TROPICAL OCEAN GLOBAL ATMOSPHERE MODELS AT THE UKMO

by

Michael Davey, Chris Gordon, Sarah Ineson and Sean Lawrence

Hadley Centre for Climate Research and Prediction
Meteorological Office
London Road
Bracknell
Berkshire RG12 2SY
U.K.

Note: This technical note is a version of the paper to be published in the proceedings of the NATO Advanced Research Workshop on Prediction of Interannual Climate Variations, held in Trieste, July 22-26, 1991.

COUPLED TOGA MODELS AT THE UKMO

Michael Davey*, Chris Gordon†, Sarah Ineson†, and Sean Lawrence‡

* Meteorological Office Unit, Robert Hooke Institute, Clarendon Laboratory, Parks Road, Oxford OX1 3PU

† Hadley Centre for Climate Prediction and Research, Meteorological Office, London Road, Bracknell, Berks RG12 2SY

‡ Oxford University Sub-Department of Atmospheric, Oceanic and Planetary Physics, Clarendon Laboratory, Parks Road, Oxford OX1 3PU

Abstract

Both general circulation (GCM) and intermediate ocean and atmosphere models are being used by the tropical ocean modelling group at the UK Meteorological Office to investigate interannual variability. A 13-year coupled GCM integration was completed in 1990, producing a realistic seasonal cycle but little interannual variability. Some details of year 8 of that integration are presented here, and a related hindcast experiment is discussed. An intermediate model with two active layers in the ocean and an equilibrium atmosphere is described: ocean climatology and preliminary coupled experiments are discussed.

1. Introduction

As part of the Tropical Ocean Global Atmosphere (TOGA) programme several numerical models are being developed and used jointly by the tropical ocean groups at the Hadley Centre at the United Kingdom Meteorological Office (UKMO) in Bracknell, and at the Hooke Institute (HI) in Oxford. The work is focussed on the Pacific region, and on the interannual variability associated with El Niño Southern Oscillation (ENSO)

events, with the aim of both understanding the mechanisms of such events and of predicting their occurrence.

ENSO events involve strong interaction of the ocean and atmosphere. It is expected that the most realistic numerical simulations of past events, and predictions of future events, will eventually be based on the detailed general circulation models that at present best represent the oceanic and atmospheric components when considered in isolation. Coupling these components together is far from straightforward however: taken separately one component behaves well when tied to the observed properties of the other, but a coupled model can easily drift into an unreasonable state when released from the observational ties. Certainly that was the case for the first coupled experiments at UKMO (Gordon 1989) and elsewhere, and subsequent work has concentrated on eliminating or neutralising such drift. For the UKMO coupled model the main early error was overheating of the western Pacific ocean that led to a permanent state like an El Niño. The specific addition of gustiness associated with convection and other general improvements to the atmospheric GCM largely overcame that defect, and led to the improved simulation described in section 2 below. A basic intercomparison of this and other coupled models has been carried out by Neelin et al. (1991).

The coupled GCMs have not yet reached the stage of making predictions, and their expense and complexity make them awkward tools to use for process studies. This gap is filled by intermediate models, which retain the main dynamical processes thought to be relevant to ENSO but in a greatly reduced form. These models reveal various ways that ENSO events may begin and evolve (see e.g. Anderson & McCreary (1985), the linear model by Hirst (1986), Schopf & Suarez (1988) and others), and when used to describe perturbations from climatology such models can have substantial predictive skill (notably Cane et al. (1986)). The first such UKMO/HI model had a single-active-layer ocean and a time-dependent atmosphere, and produced eastward propagating coupled interannual modes. In a version with active Pacific, Atlantic and Indian oceans this interannual activity was found to be confined to the Pacific region, and was strongly influenced by conditions over the land masses (Budin & Davey 1990). As a continuation of that project, a two-layer ocean with better climatology has been developed as described in section 3 below, and initial experiments with a simple equilibrium atmosphere have been carried out.

2. The coupled GCM

The present TOGA coupled GCM used at the UKMO has been developed over

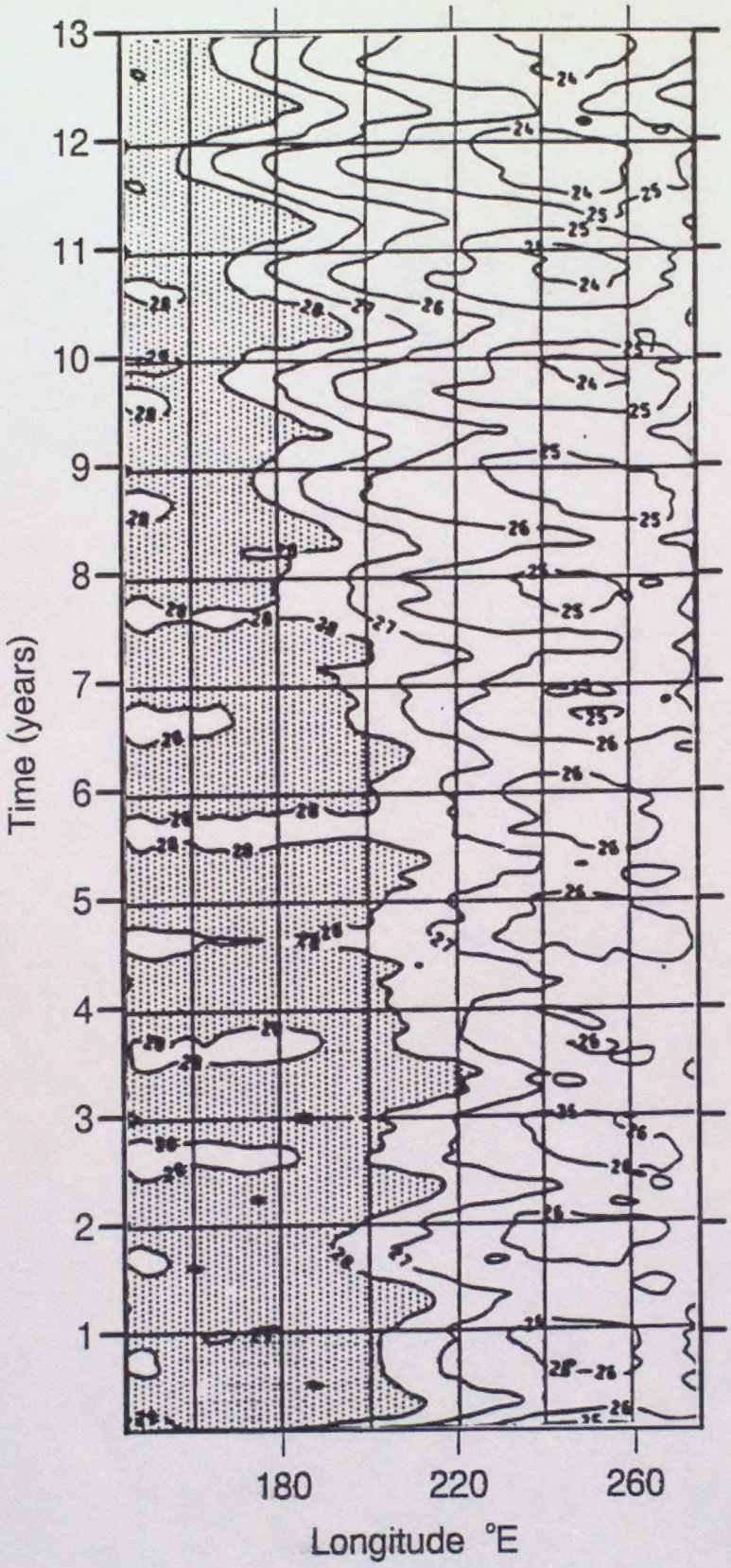

Fig. 1: Pacific equatorial sea surface temperature (°C), averaged over 5N to 5S, for 13 years from the coupled GCM. The seasonal cycle is realistic, but there is a gradual cooling trend. Temperatures greater than 28°C are stippled.

a number of years. The atmospheric component is the standard global one used for climate modelling at the UKMO, with 2.5° x 3.75° latitude-longitude resolution, and 11 vertical levels. The version used for the experiment described here includes effects such as interactive cloud specified via an explicit cloud liquid water scheme: see Slingo (1985) for a description of the basic model, and Slingo et al. (1989) and Smith (1990) for recent improvements. The ocean component is a version of the Bryan & Cox model (Cox 1984), covering the Pacific from 30°N to 30°S. Meridional resolution varies from 0.33° at the equator to 1° at the open north and south boundaries, while zonal resolution is 1.5°, reducing to 0.5° near the coasts, and there are 16 vertical levels. Simulations using the ocean model alone have been described by Gordon & Corry (1991).

The coupled experiment presented here was carried out by Gordon and Ineson in 1990. For the ocean component an energy balance mixed-layer model was embedded (c.f. Kraus & Turner 1967), to supplement the K-theory scheme (Pacanowski & Philander 1981) used previously. For the atmosphere, evaporation in convective regions was increased by adding a parameterisation of gustiness (Gordon, private communication).

The ocean is first spun up from rest, from initial climatological temperature and salinity (Levitus 1982), using wind stresses and heat fluxes obtained from the atmospheric GCM forced by climatological sea surface temperature (SST). Surface temperature and salinity are kept close to climatological values during the spinup period of over 3 years. The ocean is then fully coupled to the atmosphere. No 'flux correction' terms to overcome climate drift (see e.g. Sausen et al. 1988) are included.

Fig. 1 shows equatorial sea surface temperature T (averaged from 5°N to 5°S) during the coupled integration. The seasonal cycle is generally quite well simulated, with a pattern close to that observed. Temperature variation in the east Pacific is somewhat weak however, and there is a long-term cooling trend indicating slow climate drift. The ocean is initially too warm, and has become too cool by the end of the run. There is also some inter-annual variability, but much smaller than that associated with observed ENSO events, and there is no sign of spontaneous ENSO development.

Although no ENSO event appeared, this integration does represent a self-consistent ocean-atmosphere simulation that behaved well. SST for year 8 is close to climatological values, so we shall consider here some aspects of the simulation for that year.

From the difference shown in Fig. 2 between the equatorial model SST and the observed monthly SST climatology (here denoted T_c, taken from the COADS dataset by Woodruff et al. 1987) we see that the eastern cold tongue in the model is too cool in northern spring, and too warm in autumn. The observed SST is warmer in spring than in autumn, so this difference reflects a lack of model variability in this region, which is related to weakness of the model SE trade winds there, particularly in autumn. Further, there is little variation in the depth of the 20°C isotherm, which fluctuates between $60m$

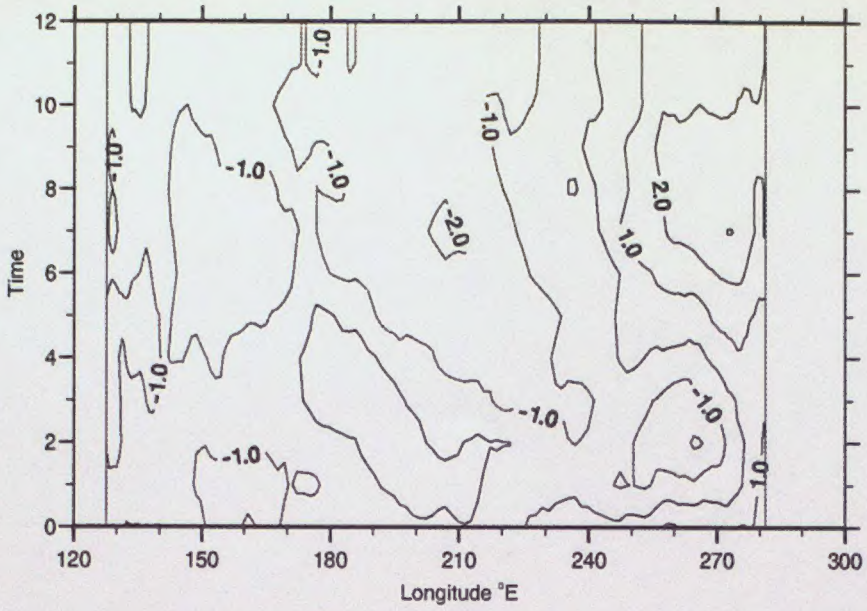

Fig. 2: Equatorial sea surface temperature difference: coupled GCM (year 8) minus climatological values from the Comprehensive Ocean-Atmosphere Data Set. Minimum −2.2°C, maximum 3.0, contour interval 1.

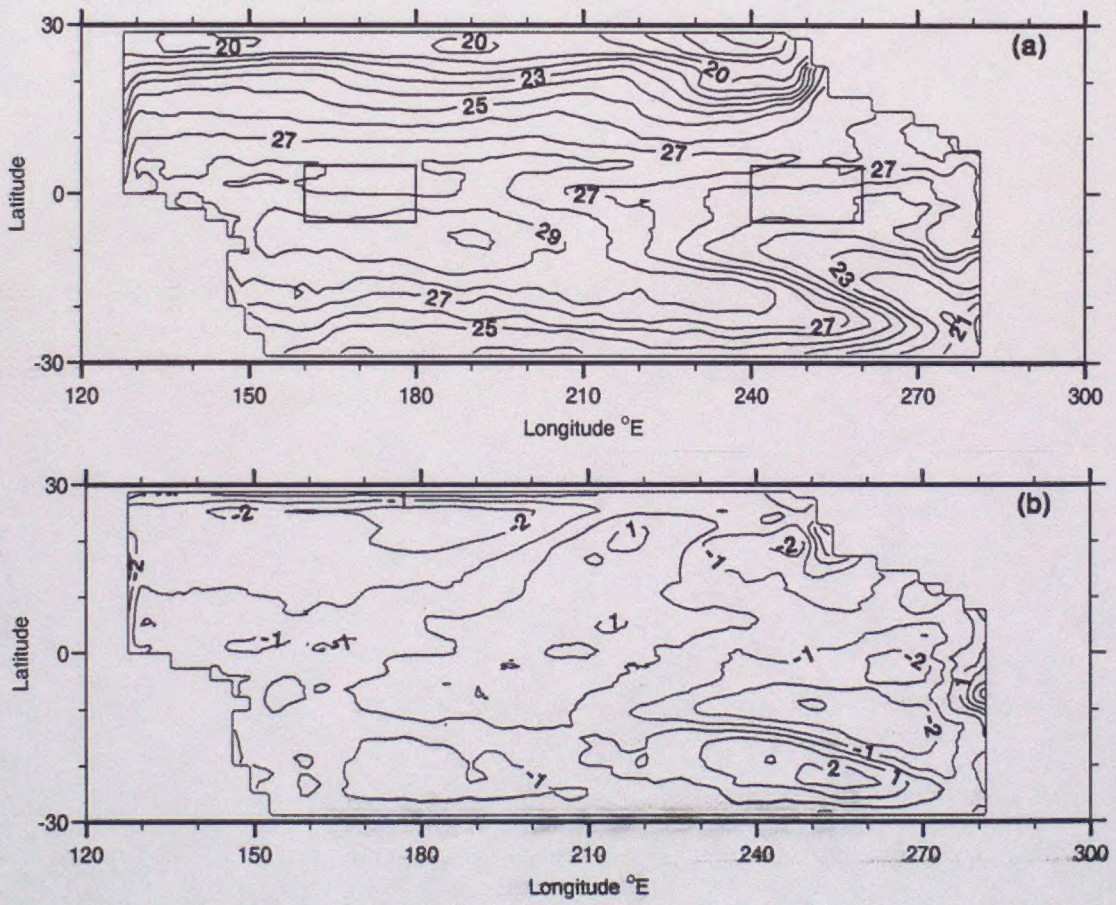

Fig. 3: Ocean surface temperatures for March of year 8 from the coupled GCM. (a) model SST, maximum 30.2°C, minimum 16.4, contour interval 1. The rectangular regions drawn in the west and east Pacific indicate areas used for the scatter plots in Figs. 4 and 5. (b) SST difference (model - COADS climatology), maximum 4.5 on South American coast, minimum -3.4, contour interval 1.

and $80m$ in the equatorial east Pacific.

The spatial patterns of T and $T - T_c$ are given for March in Fig. 3. The difference is small over most of the Pacific region, with the largest (warm) anomaly appearing off the coast of S. America, and errors of $\pm 2°$ in the SE Pacific.

The net heat flux Q into the ocean is generally small in the west Pacific (typically $20 Wm^{-2}$), increasing to over $100 Wm^{-2}$ in parts of the equatorial east Pacific. Fig. 4 gives scatter plots of Q vs. T for the two equatorial regions outlined in Fig. 3a, one just west of the dateline and the other in the east Pacific. For the western region (Fig. 4a) the relation is surprisingly linear, with a dQ/dT slope of about $-35 Wm^{-2}K^{-1}$, whereas in the eastern region (Fig. 4b) with cooler SST there is greater scatter with a tendency for positive (negative) dQ/dT for lower (higher) temperatures. Scatter plots for the heat flux components were also made: Fig. 5 shows the sensible+latent+infrared flux (dominated by the latent heat component), and the net solar flux vs. SST, for the western region. Where SST is above 28°C cloud shading (not shown) reduces the solar component substantially, but this is compensated by reduced evaporative cooling, despite the increased gustiness factor associated with precipitation there. The near-linear net relation may be fortuitous: there is somewhat more scatter in the corresponding September plot (not shown) for example. K.-M. Lau (private communication) has suggested that the relation could also be a property of the type of convection scheme used in the atmospheric GCM.

Using the above integration as a control, hindcasts of the 1982-83 ENSO event using the coupled GCM were attempted. In previous experiments the Pacific ocean GCM alone had been spun up using climatological winds (taken from the atmospheric GCM alone with climatological SST), and also using windstress for the 1980s provided by Florida State University (called FSU pseudostress, c.f. Goldenberg & O'Brien 1981). For the hindcasts the ocean component was initialised by calculating the September 1982 difference between the ocean-only integrations with climatological and FSU stresses, and adding that difference to the ocean state in the coupled integration at September of year 8. In this way a realistic complete ocean anomaly is added to a balanced ocean-atmosphere system, giving a substantial warm SST anomaly in the central Pacific. In the 82/83 ENSO event this anomaly was observed to spread eastward in the following months. In the model hindcast experiment however the warm anomaly rapidly decayed, due to strong easterly surface winds induced east of that region that caused strong surface cooling. The general structure of the atmospheric response to the anomaly was unsatisfactory, with quite different wind anomalies appearing above and within the boundary layer, for reasons that remain unclear. For some hindcasts the atmosphere was allowed to adjust to the new surface conditions before coupling, but results were essentially the same as were found without this period of adjustment.

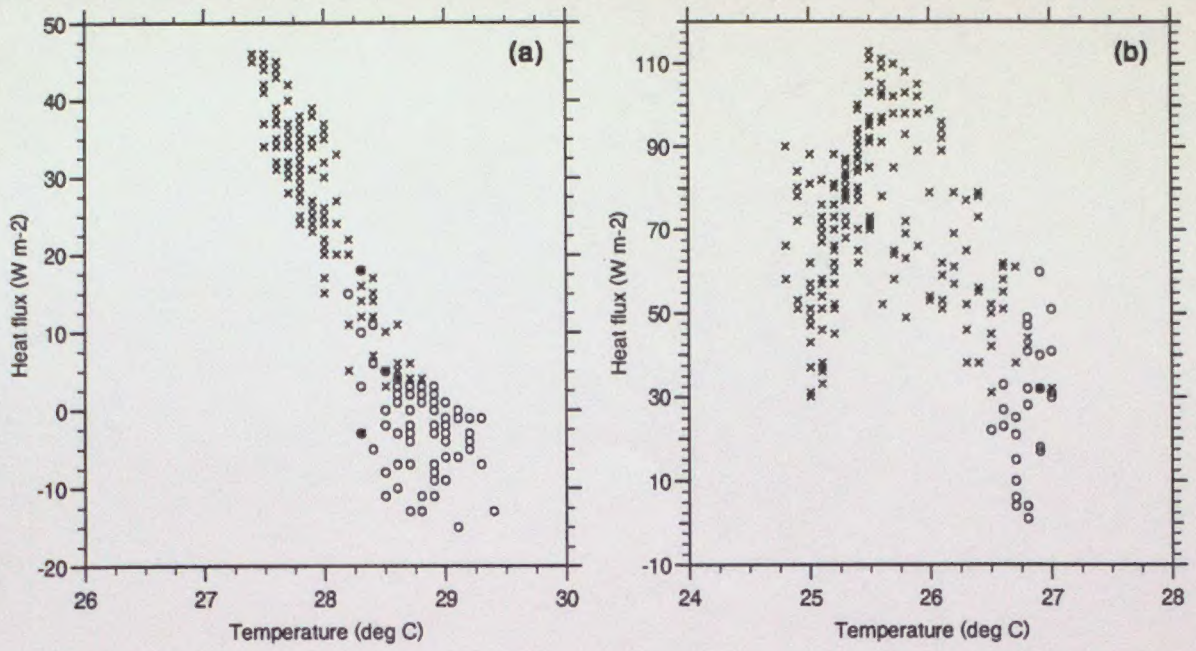

Fig. 4: Scatter plots of net surface heat flux Q into the ocean against sea surface temperature, for the March average of year 8 from the coupled GCM, for the regions shown in Fig. 3a. The symbol o is used where the model rainfall rate is greater than 10 mm/day, $\times$ otherwise, for ocean model gridpoints in the region. (a) In the west Pacific area (5S to 5N, 160E to 180E) the relation is almost linear, with a slope of $-35 W m^{-2} K^{-1}$. (b) For the east Pacific area (5S to 5N, 240E to 260E) there is more scatter, with Q increasing with SST at the lower end of the SST range.

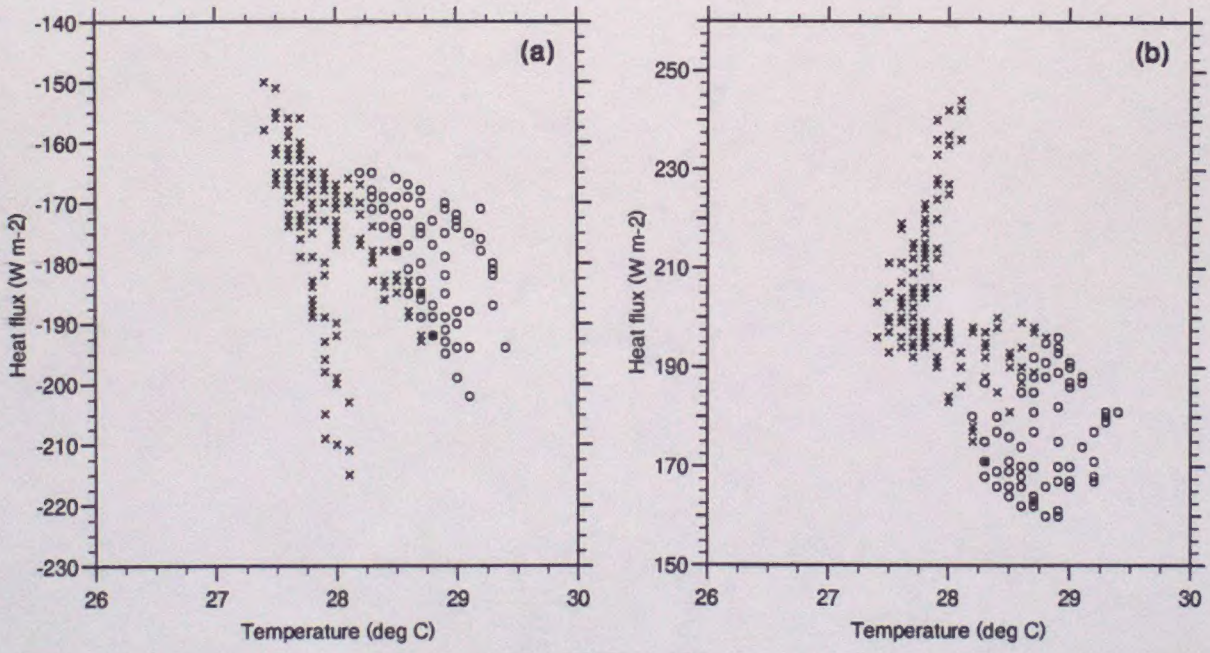

Fig. 5: Scatter plots of components of the heat flux Q into the ocean against sea surface temperature, for the March average of year 8 from the coupled GCM, for the west Pacific region 5S to 5N, 160E to 180E. The symbol o is used where the model rainfall rate is greater than 10 mm/day, $\times$ otherwise, for ocean model gridpoints in the region. (a) Sensible+latent+infrared vs. SST: the latent heat flux term is the main component. (b) Solar vs. SST: the solar component decreases where SST is largest because precipitation and cloud shading is active there.

3. Intermediate model

The reduced-physics intermediate coupled model of Budin & Davey (1991) contained an ocean with a thick single active layer. The thickness of the layer made the thermal response of the ocean rather sluggish, as found in experiments with added high frequency noise in the atmosphere, and model ocean currents could only represent an average over the depth of that layer. A new ocean model with two active layers, which could represent both surface currents and undercurrents, is being developed as described below.

3.1 Ocean equations

The ocean has two active layers with varying depth, linearised about a basic state with layer depths $\bar{h}_1$ and $\bar{h}_2$, and temperatures $\bar{T}_1$ and $\bar{T}_2$. Below the second layer the temperature is $\bar{T}_3$. The ocean dynamic equations are standard (c.f. the nonlinear model by McCreary & Kundu 1988):

$$\frac{\partial \underline{u}_1}{\partial t} + f\underline{k}\mathrm{x}\underline{u}_1 = -\frac{1}{\rho_0}\nabla p_1 + \nu\nabla^2\underline{u}_1 - d_1(\underline{u}_1 - \underline{u}_2) + \frac{\underline{\tau}}{\rho_0 \bar{h}_1} \tag{1}$$

$$\frac{\partial \underline{u}_2}{\partial t} + f\underline{k}\mathrm{x}\underline{u}_2 = -\frac{1}{\rho_0}\nabla p_2 + \nu\nabla^2\underline{u}_2 + d_2(\underline{u}_1 - \underline{u}_2) \tag{2}$$

$$\frac{\partial h_1}{\partial t} + \bar{h}_1\nabla.\underline{u}_1 = w_{e1} + w_{d1} \tag{3}$$

$$\frac{\partial h_2}{\partial t} + \bar{h}_2\nabla.\underline{u}_2 = -w_{e1} - w_{d1} + w_{e2} + w_{d2} \tag{4}$$

An equatorial beta-plane $f = \beta y$ is used. The positive terms w_{e1} (entrainment from layer 2 into layer 1) and w_{e2} (from the deep ocean into layer 2) are used to limit shallowing of each layer. They act only when a layer depth is less than some critical value h_e, giving entrainment that is roughly proportional to the square of $h_e - h$. Entrainment into the upper layer may be regarded as a crude parameterisation of the effect of wind mixing penetrating into layer 2. Similarly, negative detrainment terms w_{d1} and w_{d2} are active when layer depths exceed critical depths h_d, and are needed to allow the total volume of a layer to reach equilibrium by returning water gained by entrainment. The entrainment/detrainment algorithm also allows detrainment from layer 1 to layer 2 when layer 2 is too shallow, in preference to entrainment from the deep ocean.

Temperature is held fixed in the pressure gradient terms:

$$\frac{1}{\rho_0}\nabla p_1 = g\alpha[(\bar{T}_1 - \bar{T}_2)\nabla h_1 + (\bar{T}_2 - \bar{T}_3)\nabla(h_1 + h_2)] \tag{5}$$

$$\frac{1}{\rho_0}\nabla p_2 = g\alpha(\bar{T}_2 - \bar{T}_3)\nabla(h_1 + h_2) \quad . \tag{6}$$

Thus $\underline{u}_1$, $\underline{u}_2$, h_1 and h_2 are determined entirely by the windstress, and are independent of any temperature variations. The windstress is calculated from either monthly climatology (0.75 Hellerman stress, Hellerman & Rosenstein 1983), or FSU pseudostress multiplied by drag coefficient C_D and air density $1.2Kg\ m^{-3}$.

The flux-form thermodynamic equation for layer 1 is

$$\frac{\partial(h_1 T_1)}{\partial t} + \nabla.(\bar{h}_1 T_1 \underline{u}_1) = \frac{Q}{\rho_0 c_p} + A_T h_1 \nabla^2 T_1 + w_{e1} T_2 + w_{d1} T_1 \quad . \tag{7}$$

Originally the thermodynamic equation for layer 2 had the same form:

$$\frac{\partial(h_2 T_2)}{\partial t} + \nabla.(\bar{h}_2 T_2 \underline{u}_2) = A_T h_2 \nabla^2 T_2 - w_{e1} T_2 - w_{d1} T_1 + w_{e2} T_3 + w_{d2} T_2 \quad . \tag{8}$$

This form was chosen to conserve the total heat content of the two layers in the absence of Q, w_{e2} and w_{d2}, and to allow undercurrent advection of warm water from the west Pacific to influence the temperature of water upwelled in the east Pacific. The model took many years to reach thermal equilibrium however, so the layer 2 temperature was instead held fixed in the cases described below, with $T_2 = 23°\mathrm{C}$. Effectively this fixes the temperature of water entrained into layer 1; T_2 has no other role in this model.

The equation governing T_1 can also be expressed as

$$\frac{\partial(T_1)}{\partial t} + (\bar{h}_1/h_1)\underline{u}_1.\nabla T_1 = \frac{Q}{\rho_0 c_p h_1} + A_T \nabla^2 T_1 + w_{e1}(T_2 - T_1)/h_1 \quad , \tag{9}$$

and this is the version is used in numerical integrations. The surface heat flux Q is linearised about climatological values Q_c, with

$$Q = Q_c - \left(\frac{dQ}{dT}\right)_c (T_c - T_1) \quad , \tag{10}$$

where Q_c and sea surface temperature T_c are taken from the COADS monthly climatology and $(dQ/dT)_c$ is as calculated by Oberhuber (1988).

The equations are solved on a variable C-grid for the tropical Pacific ocean, with uniform $\Delta x = 1.5°$ longitude and Δy varying from $\Delta y_0 = 0.59°$ at the equator to 2° at the solid walls near 30°N and 30°S. (The latitudinal resolution is just half that used for

the ocean GCM in the coupled experiment described in section 2.) The viscosity varies as $A_M = A_{M0}\Delta y/\Delta y_0$.

Parameters for the experiments described below are:

$\bar{T}_1 = 28°C$	$\bar{T}_2 = 20°C$	$\bar{T}_3 = 12°C$
$\bar{h}_1 = 100m$	$\bar{h}_2 = 150m$	
$h_{1e} = 40\ m$	$h_{2e} = 40\ m$	
$h_{1d} = 200\ m$	$h_{2d} = 500\ m$	
$d_1 = 5.8\text{x}10^{-8} sec^{-1}$	$d_2 = (\bar{h}_1/\bar{h}_2)d_1$	
$A_M = 2000 m^2 sec^{-1}$	$A_T = 2000 m^2 sec^{-1}$	
$C_D = 1.15\text{x}10^{-3}$	$\alpha = 2.5\text{x}10^{-4}$	

The characteristic wave speeds for the two internal modes are $c_1 = 2.43 msec^{-1}$ and $c_2 = 0.99 msec^{-1}$. Generally only mass exchange between layer 1 and layer 2 is active: under these conditions the faster mode is very lightly damped, while the slower mode is strongly damped in regions of active upwelling.

3.2 Ocean climatology

The model was forced for several years, using 0.75 of the monthly Hellerman climatology for the wind stress $\underline{\tau}$. Fig. 6 shows the resulting equatorial temperature cycle for one year, for T_1 and $T_1 - T_c$. In the central and west Pacific there is no upwelling into layer 1. Advection effects are small in the western region, and there T_1 is effectively driven locally by the surface heat flux. In the east Pacific, where the upper layer is shallow and entrainment w_{e1} is active, upwelling of 23° water counteracts the surface heat flux to maintain the equatorial cold tongue. This cool water is then advected westward into the central region.

The simple thermodynamics used here, with the temperature of upwelled water kept constant, tends to produce eastern SST that is up to 2° too cool in northern spring (Fig. 6b) when upwelling is strongest. A warm patch appears around 230E (130W) in May and June, but then rapidly fades to be replaced by a weak cool anomaly.

The spatial SST structure at the end of March is shown in Fig. 7: temperatures in the equatorial region at this time are generally close to T_c. The largest tropical anomalies are in the eastern region, with the narrow equatorial cold tongue being about 1° too cool, and substantial warm anomalies next to the S. American coast. The corresponding currents $\underline{u}_1$ and $\underline{u}_2$ are shown in Fig. 8, with prominent zonal equatorial currents and undercurrents with magnitude about $0.3m\ sec^{-1}$, similar to the observed average currents (Wyrtki & Kilonsky 1984).

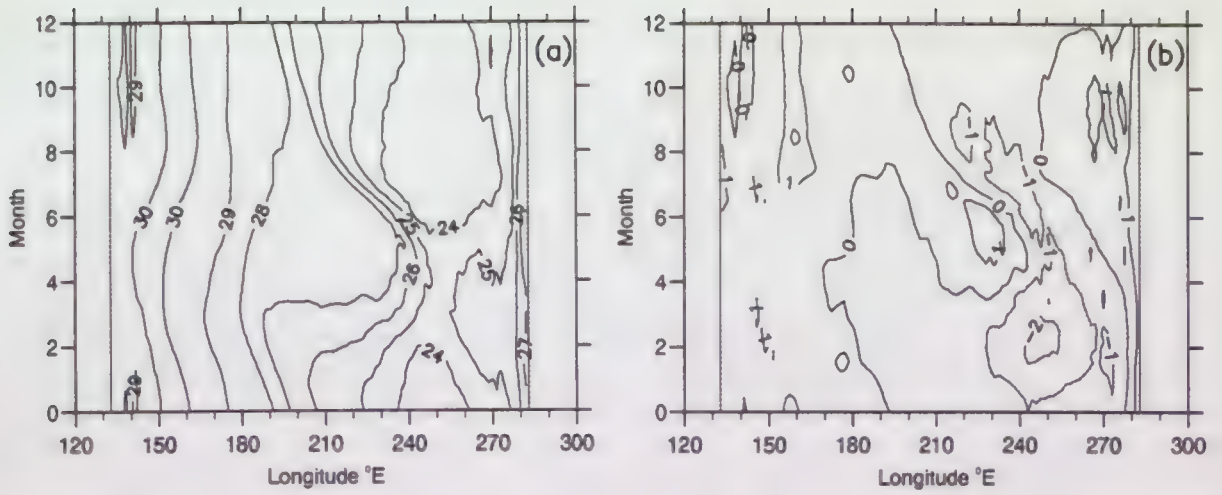

Fig. 6: The annual cycle in equatorial sea surface temperature for the intermediate ocean model forced by 0.75 Hellerman wind stress. (a) T_1, maximum 30.3°C, minimum 23.2, contour interval 1. (b) The difference $T_1 - T_c$, where T_c is calculated from the COADS climatology. Minimum -2.3, maximum 1.8, contour interval 0.5 .

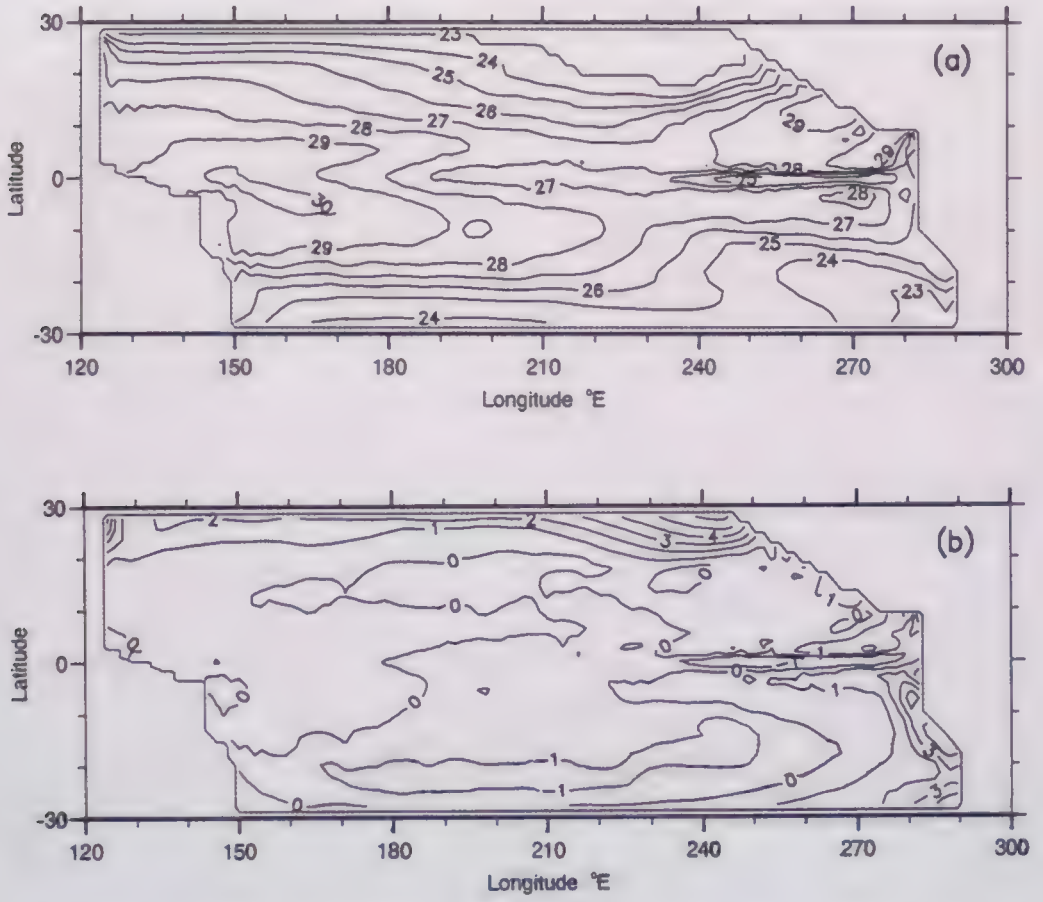

Fig. 7: Sea surface temperatures for April 1 from the intermediate ocean model forced by 0.75 Hellerman wind stress. (a) T_1, maximum 30.2°C, minimum 23.0, contour interval 1 . (b) The difference $T_1 - T_c$, where T_c is calculated from the COADS climatology. Maximum 6.3 in the north-east corner, minimum -2.0, contour interval 1.

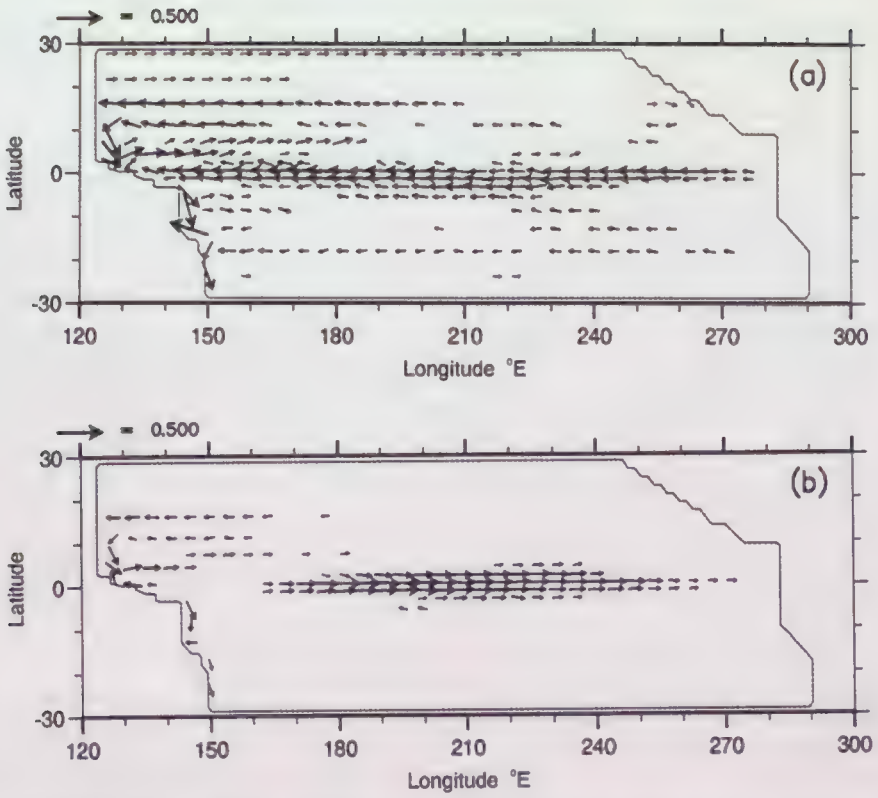

Fig. 8: Currents for April 1 from the intermediate ocean model forced by 0.75 Hellerman monthly wind stress climatology. (a) upper layer $\underline{u}_1$, maximum speed $0.45m\ sec^{-1}$. (b) lower layer $\underline{u}_2$, maximum speed 0.42 .

3.3 The ocean response to 1980-1988 winds

The ocean model was next forced with the FSU winds, first by spinning up with an average of the 1980-1988 winds, then with the monthly winds from 1980 to 1988. The climatological heat flux formulation (10) was retained. The equatorial SST is given in Fig. 9: in 1982-1983 28° water spreads from the west across to the east, as westward surface currents weaken and the upper layer deepens in the east Pacific to restrict upwelling of cool water into the upper layer. The equatorial cold tongue reappears rapidly and strongly near the end of 1983. In 1987 warm water again extends to the east Pacific, but 28° water only appears briefly there. The general pattern is similar to the observed ENSO events, but eastern sea surface temperatures are not as high as observed.

The two ENSO events show more clearly in the evolution of upper layer depth perturbation along the equator (Fig. 10). In response to the weakening easterly winds, the upper layer rapidly deepens in the east to shut off entrainment there during the two events.

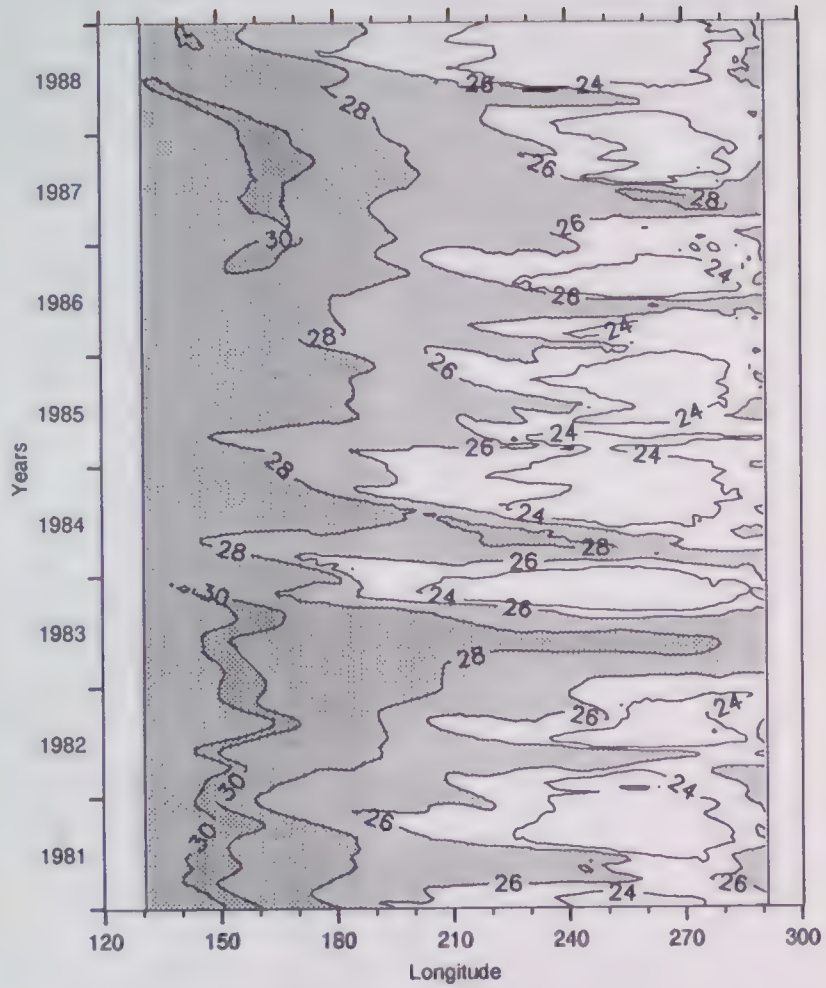

Fig. 9: Equatorial sea surface temperature T_1 for 1981 to 1988 from the intermediate ocean model forced by FSU pseudostress. Temperatures greater than 26°C are shown stippled. Maximum 30.3°C, minimum 23.0, contour interval 1.

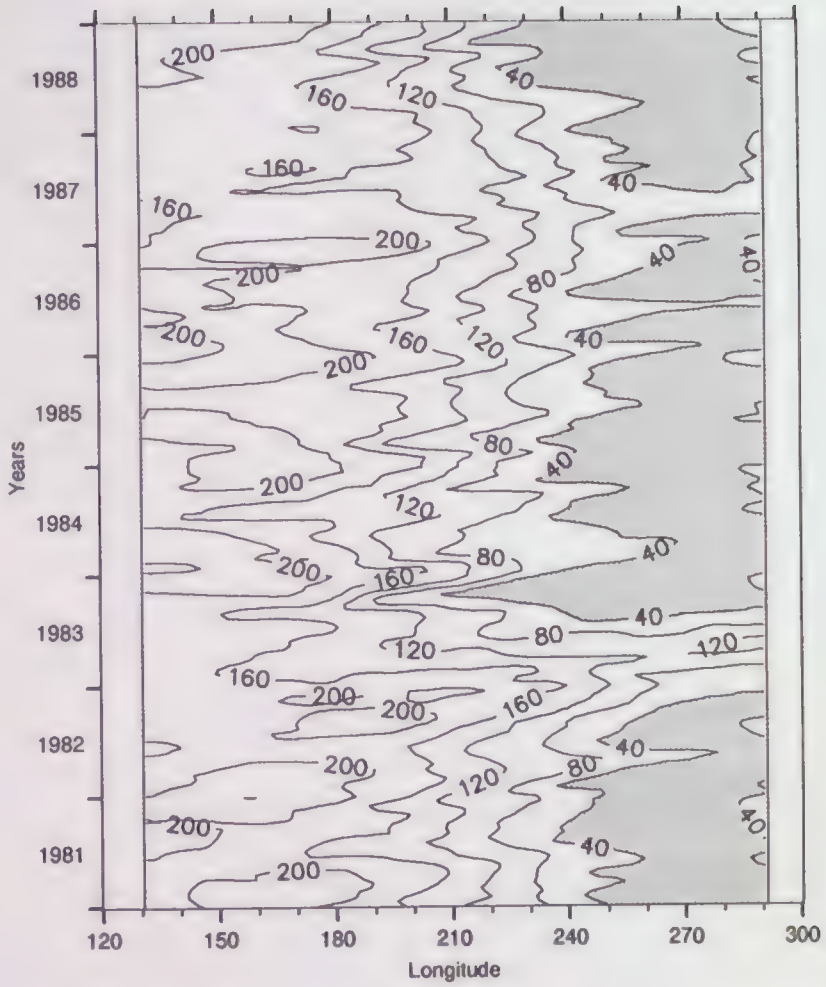

Fig. 10: Equatorial upper layer depth h_1 for 1981 to 1988 from the intermediate ocean model forced by FSU pseudostress. Maximum $240m$, minimum $26m$, contour interval $40m$. Entrainment from the lower layer to this layer occurs only in the stippled area where $h_1 < 40m$.

3.4 Preliminary coupled experiments

Sea surface temperature perturbations from the seasonal cycle described in section 3.2 above were used to force a simple equilibrium atmosphere model, to obtain surface wind perturbations $\underline{U}'$. The equations for the atmosphere have the dry shallow-water form (c.f. Gill 1980):

$$f\underline{k}\mathrm{x}\underline{U}' = -\nabla\Phi' - \epsilon\underline{U}' \tag{11}$$

$$c^2\nabla.\underline{U}' = -{Q_a}' - \epsilon\Phi' \quad , \tag{12}$$

with $c = 60msec^{-1}$ and $\epsilon = 4\mathrm{x}10^{-6}sec^{-1}$.

In the case described below the perturbation atmospheric thermal forcing ${Q_a}'$ is determined only by sea surface temperature changes, with no convergence feedback. The forcing is

$${Q_a}' = K_1[(T_1 - 28)_+ - (T_{cm} - 28)_+] + K_2(T_1 - T_{cm}) \quad , \tag{13}$$

where T_{cm} is the model SST from the climatology experiment above, and the subscript $+$ indicates that only positive values of the bracketed quantity are used. The term with coefficient K_1 represents heating by deep convection where SST exceeds $28°C$ (c.f. Anderson & McCreary 1985).

The wind stress perturbation thus obtained is added to the climatological stress used to force the ocean model:

$$\underline{\tau}' = K_T\underline{U}' \quad , \tag{14}$$

with $K_T = 8.5\mathrm{x}10^{-3}$, for stress in $N\ m^{-2}$ and wind in $m\ sec^{-1}$.

Experiments were carried out by coupling the perturbation atmosphere (every 10 days) after spinning up the ocean seasonal cycle. Residual spinup, and small errors in interpolating the saved values T_{cm}, gave small Q' for the first few months after coupling. Various values for K_1 and K_2 have been tried. For $K_1 = K_2 = 2\mathrm{x}10^{-3}\ W\ m^{-2}K^{-1}$ perturbations remained negligibly small, whereas with $K_1 = K_2 = 8\mathrm{x}10^{-3}$ perturbations grew to an unrealistic size, with strong coupled biennial oscillations. For $K_1 = K_2 = 4\mathrm{x}10^{-3}$ small cold SST anomalies in the east caused easterly wind perturbations that in turn led to seasonal extension westward of the cold tongue, a little further each year. After 8 years of this behaviour the system settled into a regular annual cycle with substantial perturbations from the uncoupled climatology. Fig. 11 shows two cycles of equatorial SST in this case: large scale movement westward of cool water is prominent each year, with rapid changes evident across the whole Pacific. The system generally behaves like an amplified annual cycle biased toward a cold La Niña state.

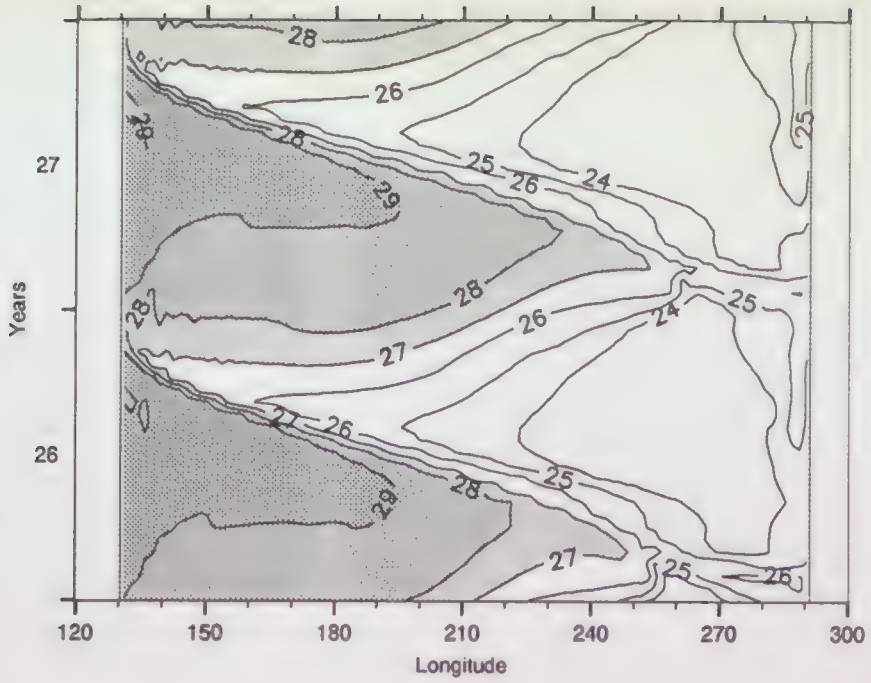

Fig. 11: Equatorial sea surface temperature T_1 for the intermediate ocean model coupled to a simple equilibrium atmosphere which is driven by perturbations from the SST climatology in Fig. 6. The coupled model has settled into an exaggerated annual cycle.

4. Future work

The present state of TOGA modelling work at the UKMO has been described. For the coupled GCM a new recoded atmospheric component will soon be available. Preliminary uncoupled SST anomaly (September 1982) tests with a trial version of the new atmosphere GCM show much better structure than was obtained in the hindcast attempts of section 2, with westerly surface wind anomalies occurring over the warm SST anomaly. The ocean GCM is being adapted for consistency with the new operating system, and ocean-only experiments will be carried out before new coupled GCM work.

Coupled experiments with intermediate models are continuing at the Hooke Institute. Allen & Davey (1991) have used an inverse atmosphere model to determine optimal parameterisations of the surface wind response to SST anomalies, and that scheme will be tested in a coupled model. Deng-Hua Wu (private communication) has added a third fixed-depth layer to a similar intermediate ocean, and if trials are successful then a third layer may be added to the ocean model described here. A hybrid model with a Pacific ocean GCM coupled to a simple equilibrium atmosphere has been developed by Stockdale (1991 D.Phil. thesis) to investigate coupled modes and to carry out ENSO hindcasts.

Acknowledgement

Ray McQuigg (UKMO) provided valuable assistance with data preparation.

References

Allen MR, Davey MK (1991) Empirical parameterisation of tropical ocean-atmosphere coupling: the 'inverse Gill' problem. Submitted to J Clim

Anderson DLT, McCreary JP (1985) Slowly propagating disturbances in a coupled ocean-atmosphere model. J Atmos Sci 42:615-628

Budin G, Davey MK (1990) Intermediate models of intraseasonal and interannual waves in the tropics. J Mar Sys 1:39-50

Cane MA, Zebiak SE, Dolan SC (1986) Experimental forecasts of El Niño. Nature 321:827-832

Cox MD (1984) A primitive equation, 3-dimensional model of the ocean. GFDL Ocean Group Tech Rep. 1, Geophys. Fluid Dyn. Lab./NOAA, Princeton, N.J.

Gill AE (1980) Some simple solutions for heat-induced tropical circulations. Q J Roy Met Soc 106:447-462

Goldenberg SB, O'Brien JJ (1981) Time and space variability of tropical Pacific wind stress. Mon Weath Rev 109:1190-1207

Gordon C (1989) Tropical ocean-atmosphere interactions in a coupled model. Phil Trans Roy Soc London A329:207-223

Gordon C, Corry RA (1991) A model simulation of the seasonal cycle in the tropical Pacific ocean using climatological and modeled surface forcing. J Geophys Res 96:847-864

Hellerman S, Rosenstein M (1983) Normal monthly windstress over the world ocean with error estimates. J Phys Oceanog 13:1093-1104

Hirst, AC (1989) Unstable and damped equatorial modes in simple coupled ocean-atmosphere models. J Atmos Sci 43:606-630

Kraus EB, Turner JS (1967) A one dimensional model of the seasonal thermocline. Part II Tellus 19:98-105

Levitus S (1982) Climatological atlas of the world ocean. NOAA Prof. Pap. 13, Natl. Oceanic and Atmos. Admin., Boulder, Colo.

McCreary JP, Kundu PK (1988) A numerical investigation of the Somali Current during the Southwest Monsoon. J Mar Res 46:25-58

Neelin JD, Latif M, Allaart MAF, Cane MA, Cubasch U, Gates WL, Gent PR, Ghil M, Gordon C, Lau NC, Mechoso CR, Meehl GA, Oberhuber JM, Philander SGH, Schopf PS, Sperber KR, Sterl A, Tokioka T, Tribbia J, Zebiak SE (1991) Tropical air-sea interaction in general circulation models. Climate Dyn , to appear

Pacanowski R, Philander SGH (1981) Parametrization of vertical mixing in numerical models of the tropical oceans. J Phys Oceanog 11:1443-1451

Sausen R, Barthel K, Hasselmann K (1988) Coupled ocean-atmosphere models with flux correction. Climate Dyn 2:154-163

Schopf PS, Suarez MJ (1988) Vacillations in a coupled ocean-atmosphere model. J Atmos Sci 45:549-566

Slingo A (1985) Handbook of the Meteorological Office 11-layer atmospheric general circulation model. UKMO Tech Note DCTN 29

Slingo A, Wilderspin RC, Smith R.N.B. (1989) The effect of improved physical parameterizations on simulations of cloudiness and the Earth's radiation budget. J Geophys Res 94:2281-2302

Smith RNB (1990) A scheme for predicting layer clouds and their water content in a general circulation model. Q J Roy Met Soc 116:435-460

Woodruff SD, Slutz RJ, Jenne RL, Steurer PM (1987) A Comprehensive Ocean Atmosphere Data Set. Bull Amer Met Soc 68:1239-1250

Wyrtki K, Kilonsky B (1984) Mean water and current structure during the Hawaii-to-Tahiti Shuttle Experiment. J Phys Oceanog 14:242-254

CLIMATE RESEARCH TECHNICAL NOTES

CRTN 1	Oct 1990	Estimates of the sensitivity of climate to vegetation changes using the Penman-Monteith equation. P R Rowntree
CRTN 2	Oct 1990	An ocean general circulation model of the Indian Ocean for hindcasting studies. D J Carrington
CRTN 3	Oct 1990	Simulation of the tropical diurnal cycle in a climate model. D P Rowell
CRTN 4	Oct 1990	Low frequency variability of the oceans. C K Folland, A Colman, D E Parker and A Bevan
CRTN 5	Dec 1990	A comparison of 11-level General Circulation Model Simulations with observations in the East Sahel. K Maskell
CRTN 6	Dec 1990	Climate Change Prediction. J F B Mitchell and Qing-cun Zeng
CRTN 7	Jan 1991	Deforestation of Amazonia - modelling the effects of albedo change. M F Mylne and P R Rowntree
CRTN 8	Jan 1991	The role of observations in climate prediction and research. D J Carson
CRTN 9	Mar 1991	The greenhouse effect and its likely consequences for climate change. D J Carson
CRTN 10	Apr 1991	Use of wind stresses from operational N.W.P. models to force an O.G.C.M. of the Indian Ocean. D J Carrington
CRTN 11	Jun 1991	A new daily Central England Temperature series, 1772-1991. D E Parker, T P Legg and C K Folland
CRTN 12	Jul 1991	Causes and predictability of Sahel rainfall variability. D P Rowell, C K Folland, K Maskell, J A Owen, M N Ward
CRTN 13	Jul 1991	Modelling changes in climate due to enhanced CO_2, the role of atmospheric dynamics, cloud and moisture. C A Senior, J F B Mitchell, H Le Treut and Z-X Li

CLIMATE RESEARCH TECHNICAL NOTES

CRTN 14	Sep 1991	Sea temperature bucket models used to correct historical SST data in the Meteorological Office. C K Folland
CRTN 15	Aug 1991	Modelling climate change, and some potential effects on agriculture in the U.K. P R Rowntree, B A Callander and J Cochrane
CRTN 16	Aug 1991	The Boreal Forests and Climate G Thomas and P R Rowntree
CRTN 17	Aug 1991	Development of a Stratosphere-Troposphere Data Assimilation System. R Swinbank.
CRTN 18	Sep 1991	A study of asynchronous coupling using a simple climate model. M K Davey.
CRTN 19	Sep 1991	The Oceanic Carbon Cycle. N K Taylor
CRTN 20	Nov 1991	Worldwide ocean-atmosphere surface fields in Sahel wet and dry years using provisionally corrected surface wind data. M N Ward
CRTN 21	Dec 1991	Coupled tropical ocean global atmosphere models at the UKMO. M K Davey, C Gordon, S Ineson and S Lawrence